Myosin V Passing over Arp2/3 Junctions: Branching Ratio Calculated from the Elastic Lever Arm Model

Andrej Vilfan
J. Stefan Institute, Ljubljana, Slovenia

ABSTRACT Myosin V is a two-headed processive motor protein that walks in a hand-over-hand fashion along actin filaments. When it encounters a filament branch, formed by the Arp2/3 complex, it can either stay on the straight mother filament, or switch to the daughter filament. We study both probabilities using the elastic lever arm model for myosin V. We calculate the shapes and bending energies of all relevant configurations in which the trail head is bound to the actin filament before Arp2/3 and the lead head is bound either to the mother or to the daughter filament. Based on the assumption that the probability for a head to bind to a certain actin subunit is proportional to the Boltzmann factor obtained from the elastic energy, we calculate the mother/daughter filament branching ratio. Our model predicts a value of 27% for the daughter and 73% for the mother filament. This result is in good agreement with recent experimental data.

INTRODUCTION

Myosin V is a two-headed processive motor protein from the myosin superfamily, involved in different forms of intracellular transport (1,2). It has drawn a lot of attention in recent years and is now one of the best studied motor proteins. The experiments have characterized it mechanically (3–10), biochemically (11–14), optically (15–17), and structurally (18–21). These studies have shown that myosin V walks along actin filaments in a hand-over-hand fashion (15,22) with an average step size of ~35 nm, roughly corresponding to the periodicity of actin filaments (3,4,6,16,18), a stall force of ~2 pN (3), and a run length of a few microns (3,23,24). Under physiological conditions, ADP release has been identified as the time-limiting step in the duty cycle (3,11).

The Arp2/3 complex (25) initiates actin filament branching in the vicinity of a protruding edge of a cell. The complex consists of seven subunits (Arp2, Arp3, and ARPC1 through ARPC5) and is activated by WASp/Scar proteins (26). It binds to the side of one (''mother'') actin filament and initiates the nucleation of a second (''daughter'' filament), which starts growing with the fast growing end (+ end) away from the Arp2/3 complex. The mother and the daughter filament enclose an angle of 70°.

The question of what happens to a myosin V motor when it arrives at an Arp2/3-mediated actin filament junction is of interest for several reasons. First, the branching behavior is important for understanding vesicle transport in the actin cortex. And second, it is of high interest when studying the fundamental mechanism of myosin V stepping, because it represents a well defined situation in which predictions from different theoretical models can be tested against the experimental result. Our aim in this article is to use the elastic lever arm model for myosin V, which is described in detail in a previous article (27), to predict the dynamics of a myosin V motor that passes over an Arp2/3 junction. In particular, we will calculate the probabilities that a motor continues along the mother or the daughter filament.

MODEL

The idea behind the elastic lever arm model for myosin V is to describe the dimeric motor as an assembly of two identical heads, connected to each other and to the cargo-binding tail with elastic lever arms. The model allows us to derive the properties of a dimeric molecule, such as step size distribution, force-velocity relation, and processivity, from the properties of an individual head, such as geometry, chemical kinetics, and elasticity. In this respect, the approach is different from the class of discrete stochastic models, which describe the motor as a single unit (28,29).

We describe each head with a five-state mechano-chemical model, similar to that for muscle myosin (e.g., (30)), where each state (with bound ADP.Pi; ADP, pre-powerstroke; ADP, post-powerstroke; without a nucleotide; detached) is connected with a certain orientation of the lever arm, as determined with electron microscopy (18,19). The lever arms are modeled as elastic beams, connected with a flexible joint. A recent study measuring fluctuations in the position of the free head (31) has demonstrated that the lead head diffuses around the joint freely before binding to the next actin site, meaning that there is no detectable elastic energy cost connected with variation in the angle between the two lever arms. The very nature of protein flexibility, which mainly originates from the twisting of bonds between carbon atoms in the backbone, leads us to the conclusion that the joint is also fully flexible with regard to rotation of each lever arm along its axis. Similar flexibility has also been observed in myosin II (32–34).

The calculation of the branching probability is greatly simplified if we make the following assumptions. First, we

Submitted August 27, 2007, and accepted for publication December 11, 2007.

Address reprint requests to Andrej Vilfan, Tel.: 386-1-477-3874; E-mail: andrej.vilfan@ijs.si.

Editor: E. Michael Ostap.

0006-3495/08/05/3405/08 $2.00

doi: 10.1529/biophysj.107.120568

assume that the binding of the lead head always advances to a step, which means that its unbinding is significantly slower than the step that follows in the regular cycle (Pi release). Second, we assume that the probability for the lead head to bind to site j if the trail head is bound to site i is given by the Boltzmann factor

$$P_{j|i} = \frac{\exp\left(-\frac{U_{i,j}}{k_B T}\right)}{\sum_{j'} \exp\left(-\frac{U_{i,j'}}{k_B T}\right)}. \quad (1)$$

$U_{i,j}$ denotes the elastic energy of deformed lever arms when the trail head is in the post-powerstroke state, bound to site i, and the lead head in the pre-powerstroke state to site j. In the following, we will use the notation where the sites on the mother filament are marked with (M,i) and those on the daughter filament with (D,i). For example, $P_{D,2|M,-9}$ denotes the conditional probability for the lead head to bind to site 2 on the daughter filament if the trail head is bound to the site -9 on the mother filament. We enumerate the actin subunits so that the central subunit under the Arp2/3 complex on the mother filament has the index 0. Positive indices denote subunits toward the plus (+) end and negative toward the minus (−) end. Subunits of the daughter filament are enumerated from 0 onwards. Note that sites numbered -2, 0, and 2 on the mother filament are not accessible for a myosin V head, because of steric hindrance with the Arp2/3 complex.

The structure of the Arp2/3 complex and both actin filaments (Fig. 1) has been determined from electron microscopy studies (35,36) and its parameters are summarized in Table 1.

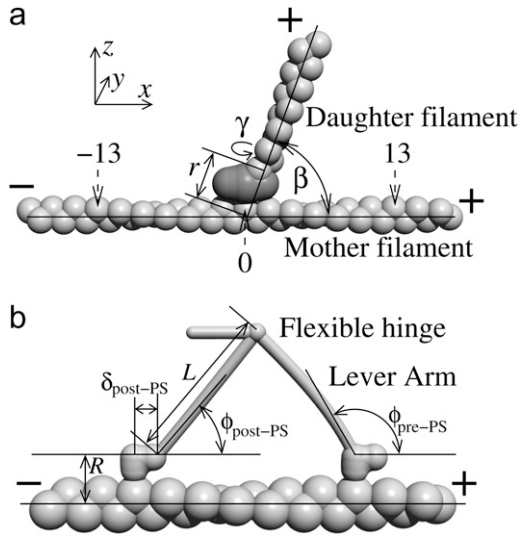

FIGURE 1 Arp2/3 junction and a dimeric myosin V motor. (*a*) The Arp2/3 complex is attached to the side of the mother filament occupying subunits -2, 0, and 2. It nucleates the growth of a daughter filament, whose position is determined by the angles β (branching angle), γ (twist), and r (distance from the first subunit to the center of the mother filament). (*b*) The myosin V motor consists of two heads, connected with lever arms, which we describe as elastic rods. The proximal end of each lever arm always leaves the head at a fixed angle ϕ, which depends on the nucleotide state of that head. The distal ends of both lever arms are connected with a fully flexible joint.

While we approximated actin with the commonly assumed 13/6 helix in the original article (27), we use a more accurate 28/13 helix here, with the angle $\theta_0 = 167.14°$ between adjacent subunits. A detailed discussion on different helix models and their consequence for the calculated step size distribution can be found in Vilfan (37).

When a head is bound to the site i, the starting point and the unit vector giving the initial direction of the lever arm are given by

$$\mathbf{x}_0 = \mathbf{R}_x(-i\theta_0)\begin{pmatrix} ia+\delta \\ 0 \\ R \end{pmatrix} \quad \hat{\mathbf{t}}_0 = \mathbf{R}_x(-i\theta_0)\begin{pmatrix} \cos\phi_i \\ 0 \\ \sin\phi_i \end{pmatrix}, \quad (2)$$

where $\mathbf{R}_x$ denotes the rotation matrix around the x axis,

$$\mathbf{R}_x(\theta) = \begin{pmatrix} 1 & 0 & 0 \\ 0 & \cos\theta & -\sin\theta \\ 0 & \sin\theta & \cos\theta \end{pmatrix}. \quad (3)$$

For a head bound to the daughter filament, the two vectors read

$$\mathbf{x}_0 = \mathbf{R}_y(-\beta)\mathbf{R}_x(\gamma - i\theta_0)\begin{pmatrix} r+ia+\delta \\ 0 \\ R \end{pmatrix}$$

$$\hat{\mathbf{t}}_0 = \mathbf{R}_y(-\beta)\mathbf{R}_x(\gamma - i\theta_0)\begin{pmatrix} \cos\phi_i \\ 0 \\ \sin\phi_i \end{pmatrix}, \quad (4)$$

with

$$\mathbf{R}_y(\beta) = \begin{pmatrix} \cos\beta & 0 & \sin\beta \\ 0 & 1 & 0 \\ -\sin\beta & 0 & \cos\beta \end{pmatrix}. \quad (5)$$

Here $\beta = 70°$ denotes the angle between the mother and the daughter filament and $\gamma = 39°$ the rotation of the daughter filament around its axis (see Fig. 1).

We calculate the shapes of both lever arms as described in Vilfan (27) by minimizing the bending energy $U = \int ds\, EI(C(s))^2/2$, where $C(s)$ denotes local curvature. For the bending modulus of the lever arm we use the value $EI = 1500$

TABLE 1 Geometric parameters of the Arp2/3 junction and a myosin V head

Parameter	Symbol	Value
Distance actin subunits	α	2.75 nm
Angle actin subunits	θ_0	167.14°
Daughter filament angle	β	70°
Daughter filament offset	r	12 nm
Daughter filament rotation	γ	39°
Lever arm start: radial position	R	8 nm
Lever arm start: displacement	δ_{pre-PS}	0
	$\delta_{post-PS}$	3.5 nm
Lever arm angle	ϕ_{pre-PS}	115°
	$\phi_{post-PS}$	50°
Lever arm length	L	26 nm

pN nm^2, which corresponds to a spring constant of $\kappa = 3EI/L^3 = 0.25$ pN/nm, measured at the tip of the lever arm. This value was originally estimated from the stall force, but it shows good agreement with direct optical tweezer measurements (38). We neglect any additional compliance resulting from the head or converter domain. Because most of the bending takes place in the proximal part of the lever arm, we expect that its effect would not be significantly different. For the temperature we use the value $T = 27°C$.

RESULTS

Stepping of myosin V in the absence of the Arp2/3 complex

When a myosin V motor is sufficiently far away from the Arp2/3 complex, it exhibits the stepping pattern that has already been discussed (27,37). We restrict the step lengths of an unperturbed motor to 11, 13, and 15 subunits, with probabilities

$$P_{11} = P_{\mathrm{M,i+11|M,i}} \approx 0.005, \tag{6}$$

$$P_{13} = P_{\mathrm{M,i+13|M,i}} \approx 0.895, \tag{7}$$

$$P_{15} = P_{\mathrm{M,i+15|M,i}} \approx 0.1, \tag{8}$$

calculated from Eq. 1. Probabilities for other step sizes, such as P_9 and P_{17} turn out to be very small. Note that, in this calculation, P_{11} and P_{15} are likely to be somewhat underestimated; their values are somewhat higher if we take into account torsional fluctuations in the actin helix (37).

The average step size can be calculated from these probabilities as

$$\bar{l} = 11P_{11} + 13P_{13} + 15P_{15} \approx 13.2. \tag{9}$$

In the absence of the Arp2/3 junction, the fraction of sites that get accessed by a passing myosin V motor is $1/\bar{l}$. This is also

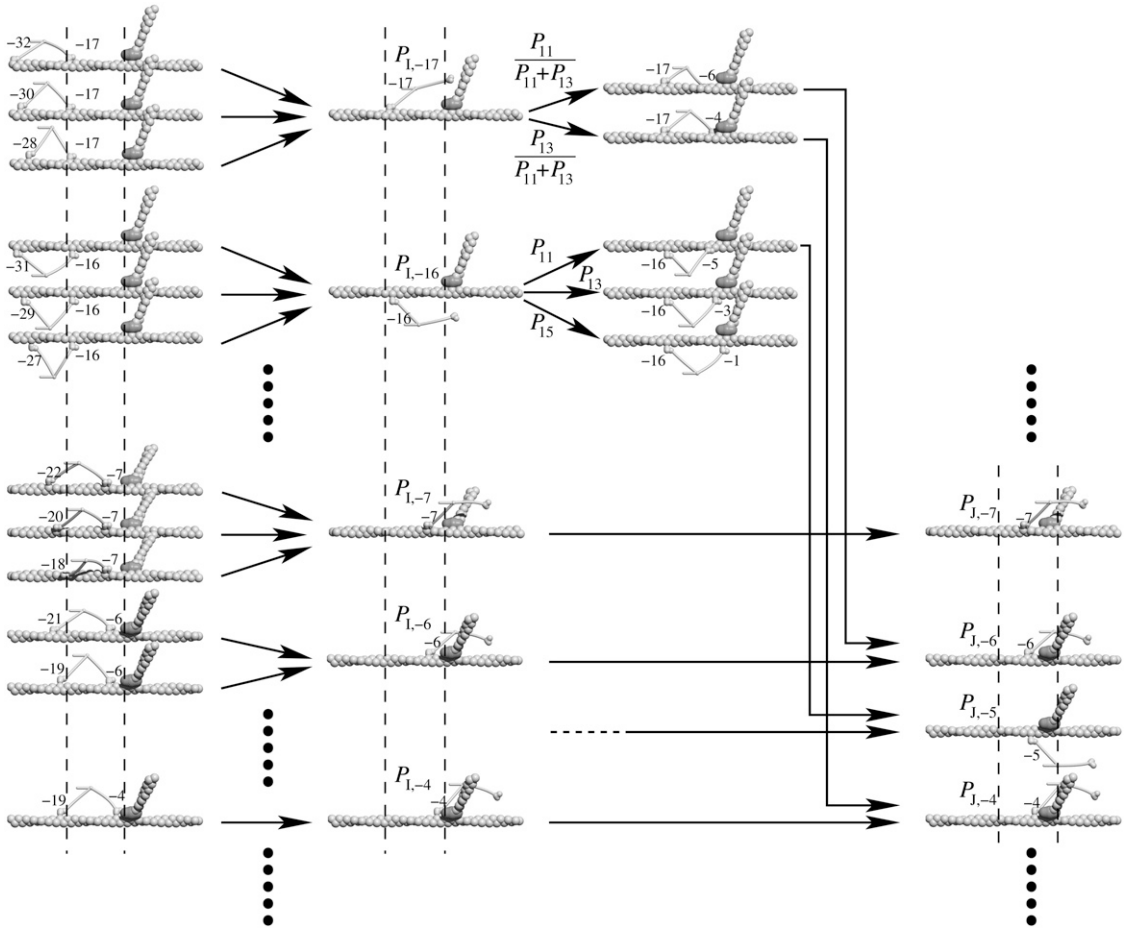

FIGURE 2 Different pathways on which a myosin V motor can approach the Arp2/3 junction. The probability distributions for the first accessed site in the two intervals marked with dashed lines are denoted as $P_{\mathrm{I,i}}$ and $P_{\mathrm{J,i}}$. $P_{\mathrm{I,i}}$ represents the probability that i is the first accessed site with $-17 \le i \le -3$ (between *dashed lines* in the *first* or *second column*). For values between -17 and -7, this state can be reached with three different step sizes. For $i = -6$ and $i = -5$, it can be reached with two different step sizes (13 and 15). If it is reached by a shorter step (11 subunits), it means that the preceding binding site was already inside the interval $-17. \ldots -3$, so i is not the first accessed site within it. For $i = -4$ and $i = -3$, the site can only be reached with a 15-subunit step. $P_{\mathrm{J,i}}$ denotes the probability that i is the first accessed subunit in the interval $-13 \le i \le 1$ (*dashed lines* in the *right column*).

the probability that a site before the junction ($i \leq -7$, as will be shown later) ever gets accessed by the motor:

$$P_{\mathrm{M,i}} = \frac{1}{\bar{l}} \quad \text{for} \quad i \leq -7. \tag{10}$$

Initial state: first accessed site in the interval $-17 \leq i \leq -3$

We start our analysis at the point where a head of an approaching myosin V first passes the subunit -17 or binds to it. This way the initial state is definitely not influenced by the presence of the Arp2/3 complex. By counting only the first accessed site in this interval, we avoid double-counting of events where the motor binds, for example, first to site -17 and then to -4.

We denote with $P_{\mathrm{I,i}}$ the probability that once the first head has bound to any subunit in the interval $-17 \leq i \leq -3$, it has happened at subunit i. $P_{\mathrm{I,i}}$ can be calculated in a way that is illustrated in Fig. 2. The sites between -17 and -7 can only be reached from outside the interval. Therefore, whenever the motor binds to one of them, it becomes the first accessed site in this interval. The probability $P_{\mathrm{I,i}}$ then equals the probability that the site i ever gets accessed by the motor, which is $1/\bar{l}$, according to Eq. 10. For $i = -6$ and higher the situation becomes different. Site -6 counts as the first site in this interval if the preceding step size is 13 or 15 subunits, but not if it is 11. Therefore, the corresponding probability is $P_{\mathrm{I},-6} = (P_{13}+P_{15})/\bar{l}$. The probability that the first site accessed in this interval is -5, $P_{\mathrm{I},-5}$, has the same value. Finally, the sites -4 and -3 will be the first accessed sites in the interval if they are following a 15-subunit step. Therefore, their probabilities are $P_{\mathrm{I},-4} = P_{\mathrm{I},-3} = P_{15}/\bar{l}$. The probabilities $P_{\mathrm{I,i}}$ are given in the second column of Table 2 and shown in the top graph of Fig. 3.

As a next step, we will derive the probability distribution $P_{\mathrm{J,i}}$ for the first accessed site in the interval $-13 \leq i \leq 1$. We choose this interval because (M,-13) is the first site from which the motor can reach the daughter filament. This distribution can be obtained from $P_{\mathrm{I,i}}$ by redistributing probabilities for sites between -17 and -14 according to the conditional probability for the next step

$$P_{\mathrm{J,j}} = P_{\mathrm{I,j}} + \sum_{\mathrm{i}=-17}^{-14} P_{\mathrm{M,j|M,i}} P_{\mathrm{I,i}}, \tag{11}$$

as shown in Fig. 3. The values of $P_{\mathrm{J,j}}$ are given in the third and fourth column of Table 2. This distribution defines the state from which we will calculate the branching ratio at the Arp2/3 junction in the following section.

Conditional branching ratio

Now we can calculate the conditional probabilities that the lead head binds to the daughter filament, if the trail head is bound to a mother filament subunit i fulfilling $-13 \leq i \leq 1$. We denote this probability as $P_{\mathrm{d|M,i}}$.

TABLE 2 Probability distribution $P_{\mathrm{I,i}}$ for the first accessed binding site in the interval $-17 \leq i \leq -3$

i	$P_{\mathrm{I,i}}$	$P_{\mathrm{J,i}}$	$P_{\mathrm{J,i}}$
-17	$1/\bar{l}$		
-16	$1/\bar{l}$		
-15	$1/\bar{l}$		
-14	$1/\bar{l}$		
-13	$1/\bar{l}$	$1/\bar{l}$	0.0758
-12	$1/\bar{l}$	$1/\bar{l}$	0.0758
⋮	⋮	⋮	⋮
-7	$1/\bar{l}$	$1/\bar{l}$	0.0758
-6	$(P_{13}+P_{15})/\bar{l}$	$(P_{13}+P_{15}+(P_{11}/P_{11}+P_{13}))/\bar{l}$	0.0759
-5	$(P_{13}+P_{15})/\bar{l}$	$1/\bar{l}$	0.0758
-4	$P_{15}/\bar{l}$	$(P_{15}+(P_{13}/P_{11}+P_{13})+1)/\bar{l}$	0.1587
-3	$P_{15}/\bar{l}$	$1/\bar{l}$	0.0758
-2		—	
-1		$(P_{15}+P_{13})/\bar{l}$	0.0754
0		—	
1		$P_{15}/\bar{l}$	0.0075

$P_{\mathrm{J,i}}$ denotes the probability distribution for the first accessed site in the interval $-13 \leq i \leq 1$. $P_{\mathrm{J,i}}$ is calculated according to Eq. 11.

Fig. 4 shows the most relevant dimer configurations with the trail head on mother filament sites between -15 and 6 and the lead head either on mother or on daughter filament. For each trail head position, the conditional probability that the lead head binds to a certain site is given by Eq. 1 with the index j' running over all accessible mother- as well as daughter-filament sites—corresponding to one row in Fig. 4. Generally speaking, the daughter filament can either be reached directly, in a one-step process such as (M,-6) → (D,3), or in a two-step process such as (M,-9) → (M,4) →

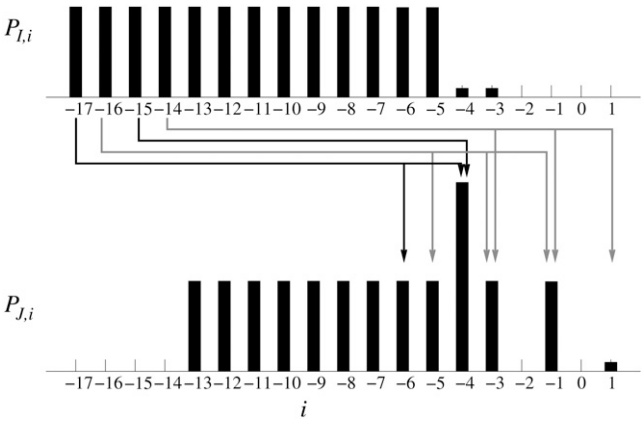

FIGURE 3 Probability distribution $P_{\mathrm{I,i}}$ (*upper diagram*) for the first accessed binding site on the mother filament in the interval $-17 \leq i \leq -3$. The lower diagram shows the probability distribution $P_{\mathrm{J,i}}$ for the first accessed site with $-13 \leq i \leq 1$. $P_{\mathrm{J,i}}$ is calculated according to Eq. 11, by redistributing the probabilities for -17 to -14 to other sites, as indicated by arrows. For example, if -17 is the first accessed site with $-17 \leq i \leq -3$, the first accessed site with $-13 \leq i \leq 1$ can either be -6 or -4. Note that the total probability that the motor binds to site -4 is higher than for any other site, which is due to the inaccessibility of site -2.

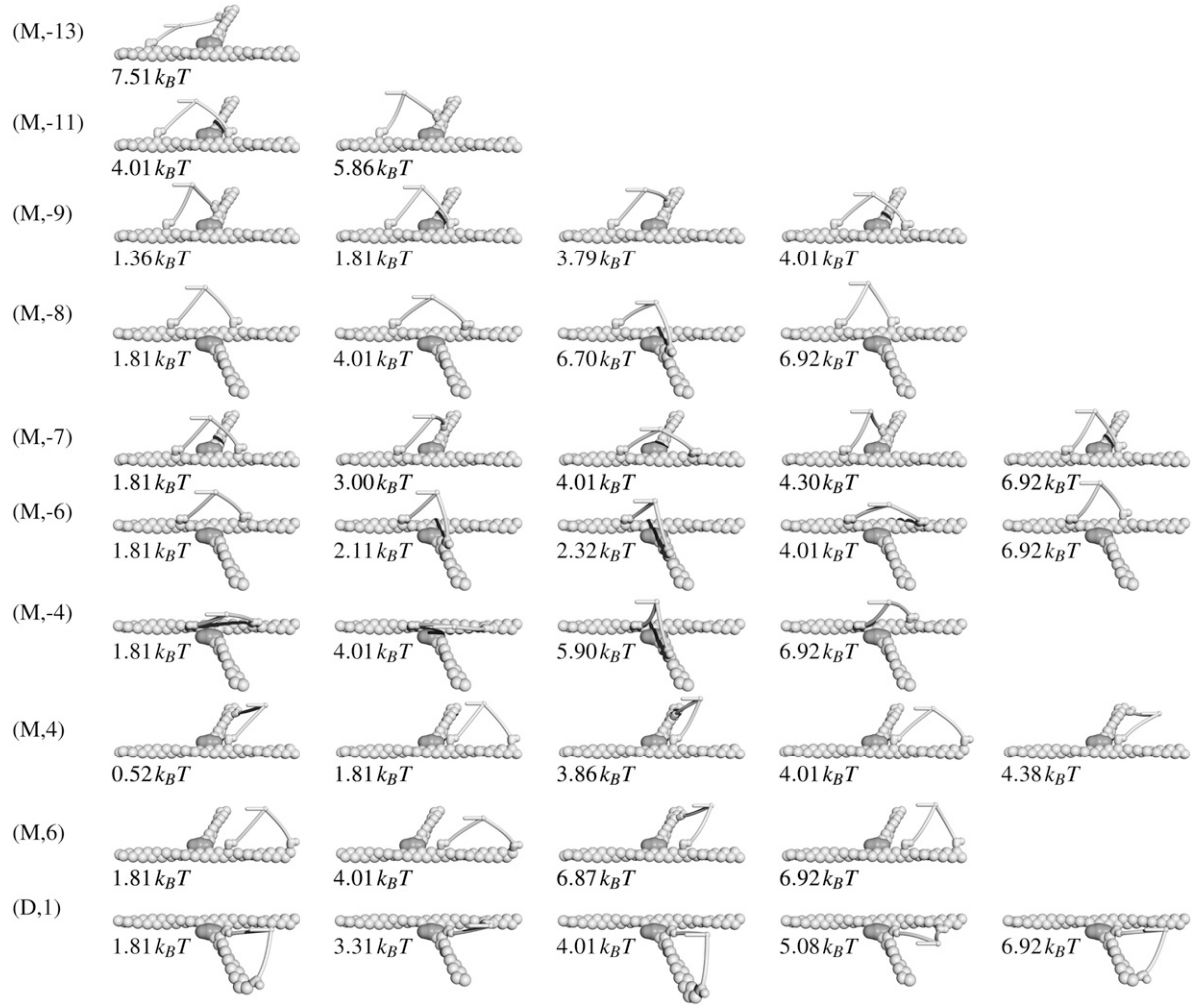

FIGURE 4 Most probable lead head binding sites for different trail head positions. For selected trail head binding sites i, a collection of lead head binding sites and their bending energies $U_{i,j}$ (in units of k_BT) is shown. Some trail head positions which do not have significant branching probabilities (e.g., −12) are omitted. The shape of both lever arms in each configuration is calculated numerically, by minimizing the bending energy.

(D,8). Two examples are shown in Fig. 5. The probability that a motor with the trail head bound to site (M,i) eventually binds to the daughter filament is

$$P_{\mathrm{d|M,i}} = \sum_{\mathrm{j}} \left(P_{\mathrm{D,j|M,i}} + \sum_{\mathrm{k}} P_{\mathrm{D,j|M,k}} P_{\mathrm{M,k|M,i}} \right). \qquad (12)$$

Here the first term denotes one-step processes and the second term two-step processes, where the motor first binds to site k on the mother filament and subsequently to site j on daughter filament. Our numerical calculation shows that the only significant terms are those with $k = 4$. The branching ratio $P_{\mathrm{d|M,i}}$ for each trail head position is shown in Fig. 6. The graph shows separately the contributions of one- and two-step processes.

Total branching ratio

With these probabilities and weights $P_{\mathrm{J,\,i}}$ we finally obtain the branching ratio for the daughter filament:

$$P_{\mathrm{d}} = \sum_{\mathrm{i}=-13}^{1} P_{\mathrm{J,i}} P_{\mathrm{d|M,i}} \approx 0.27. \qquad (13)$$

If one head binds to the daughter filament, there is still some probability that the next head will bind back to the mother filament. One such example, with the trail head on the site (D,1), is shown in the last row in Fig. 4. However, the contribution of such events to the total branching ratio is not significant.

DISCUSSION

While the exact result calculated above does require us to take into account all the individual configurations, its order of magnitude can also be understood with a simple ''hand-waving'' argument, which goes as follows. Roughly speaking, the approaching myosin V motor can either reach the Arp2/3 complex on the opposite side of the actin filament, in which case it cannot switch to the daughter filament, or on the same side—in which case the probability to switch to the

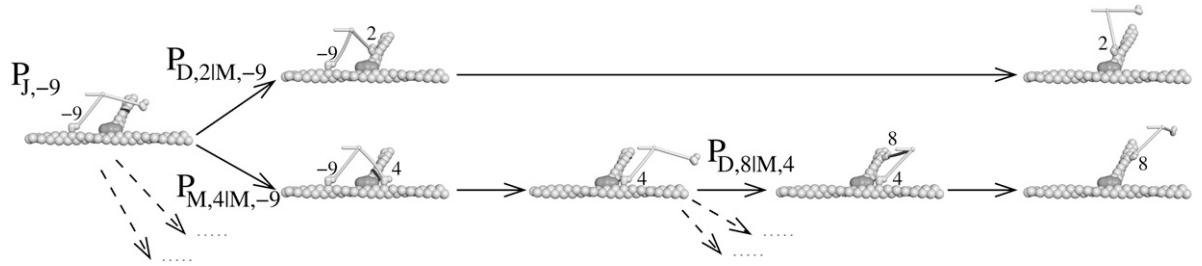

FIGURE 5 An example of a one-step (*upper path*) and two-step (*lower path*) process through which the myosin V motor can reach the daughter filament. The probability that the trail head is bound to subunit (M,−9) in the initial state is $P_{\mathrm{J},-9}$. In the next step, the lead head can bind to site (D,2) with conditional probability $P_{\mathrm{D,2|M,-9}}$. We denote such processes as one-step. Alternatively, the lead head can bind to the site (M,4) with conditional probability $P_{\mathrm{M,4|M,-9}}$ and, subsequently, the other head can bind to site (D,8) with conditional probability $P_{\mathrm{D,8|M,4}}$. This is an example of a two-step process. Note that this scheme shows just two examples of possible pathways and omits alternatives that are indicated by dashed arrows.

daughter filament is ~1/2. Together, this gives a branching ratio of 1/4, not far from the exact result of 0.27.

An experiment measuring (among other quantities) the branching ratio at Arp2/3-mediated actin filament junctions was recently carried out by Ali et al. (39). The results are not directly comparable—in the experiment, the actin filaments were attached to a glass surface so that some binding sites were not accessible for myosin V. However, because the blocked sites are different depending whether the side filament branches to the left or to the right, we expect that in statistical average, the calculated branching ratio still gives a good approximation. In the experiment 18% of the molecules dissociated, 20% continued on the daughter filament, and 62% on the mother filament. If we discount dissociation events, this means that the fraction that switched to the daughter filament was 24%. The statistical error of this figure is $\sim\pm5\%$ (the total number of events observed was 76). Therefore, the result can be considered in excellent agreement with the model calculation.

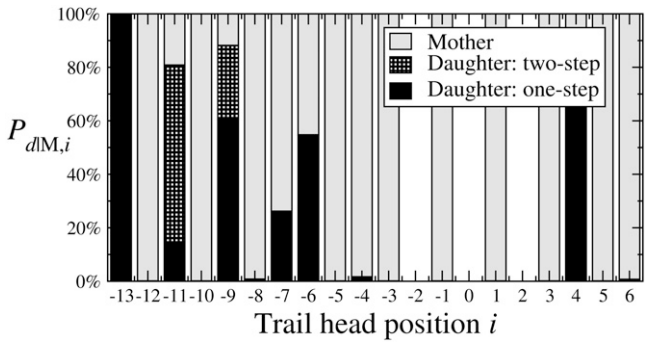

FIGURE 6 Probability that the motor will step on and continue its walk along the daughter filament if the trail head is initially bound to site i on the mother filament, $P_{d|\mathrm{M},i}$ (*solid* and *hatched bars*), as calculated from Eq. 12. The solid bars show the contribution of one-step processes, in which the lead head binds to a site on the daughter filament immediately. The hatched bars show the contribution of two-step processes in which the motor first binds to another site on the mother filament (usually site 4) and then in the second step to the daughter filament. The shaded bars show the probability that the motor continues along the mother filament.

Note that our calculation only concerns stepping patterns and does not take into account kinetics. This has an important advantage that the result only depends on geometric and elastic parameters, but not on kinetic constants, some of which are still less well known (27). Combining this model with the full kinetic scheme could influence the predicted branching ratio as follows. First, the binding rate of the lead head can be different in the vicinity of the Arp2/3 complex. And second, the ADP release rate of the rear head can be influenced by intramolecular strain, possibly also by its lateral (off-axis) component, as observed by Purcell and coworkers (40). Both these effects do not have a direct influence on the branching ratio, but they might have an indirect one by influencing the dissociation probability. In this calculation, events where the whole myosin V molecule dissociates from the actin filament are not taken into account. There is, however, evidence that the predominant dissociation path leads through detachment of a head in the ADP state (23,41)—these processes are denoted as Pathway 2 in Vilfan (27). It is therefore plausible that the termination rate increases if either the lead head is hindered in its search for a binding site, or the ADP release in the trail head is slowed down. In our model (see elastic energies in Fig. 4), the lead head binding rate is strongly reduced if the trail head is bound to site −13; it is also reduced somewhat if the trail head is bound to −11, while it is accelerated for trail head positions −9 and 4. In total, dissociation can be accelerated by the presence of the Arp2/3 junction in 2 out of $\bar{l}$ cases. Without going into quantitative details, one can conclude that the dissociation probability could theoretically increase by up to $2/\bar{l} \approx 0.15$. The branching ratio for the daughter filament could then be somewhat smaller, because those trail head positions that have the higher branching ratio are also more likely to lead to dissociation. The effect caused by the strain-dependent ADP release rate is more difficult to estimate, mainly because the exact influence of off-axis strain on the ADP release is not yet known quantitatively.

To check the robustness of our result against uncertainties in model parameters, we calculated the variation of the branching ratio with several model parameters. Note that

these calculations were carried out numerically and took into account all relevant processes, including longer and shorter steps, as well as transitions not shown in Fig. 4. Data in Fig. 7 shows a variation of $\sim\pm10\%$ if either the lead head or the trail head angle is modified by $\pm15°$. The allowed variation of these two parameters that keeps the model consistent with the experimental result is therefore restricted, although parameter sets where both angles are increased or decreased simultaneously cannot be excluded. The result is more robust against variations in the lever arm stiffness *EI*, where deviations do not exceed a few percent if the value of *EI* is changed by a factor of 3 in either direction.

We can therefore conclude that the calculated branching ratio adds support to the elastic lever arm model presented in Vilfan (27) and the geometric parameters used there. However, we cannot use it as a criterion to determine the lever arm stiffness, which is still not known precisely. Another open question is to what extent the result can be reproduced with alternative models, such as Lan and Sun (42), which uses a more complex model for the elasticity of the lever arm, with a soft longitudinal ($\sim$1/3 of the value used there), but very stiff azimuthal component. The completely different class of hotspot models, which proposes that the position of the next binding site is determined by a propagating conformational change in the actin filament (43), on the other hand, seems less compatible with the finding, unless the conformational change could propagate through the Arp2/3 complex as well.

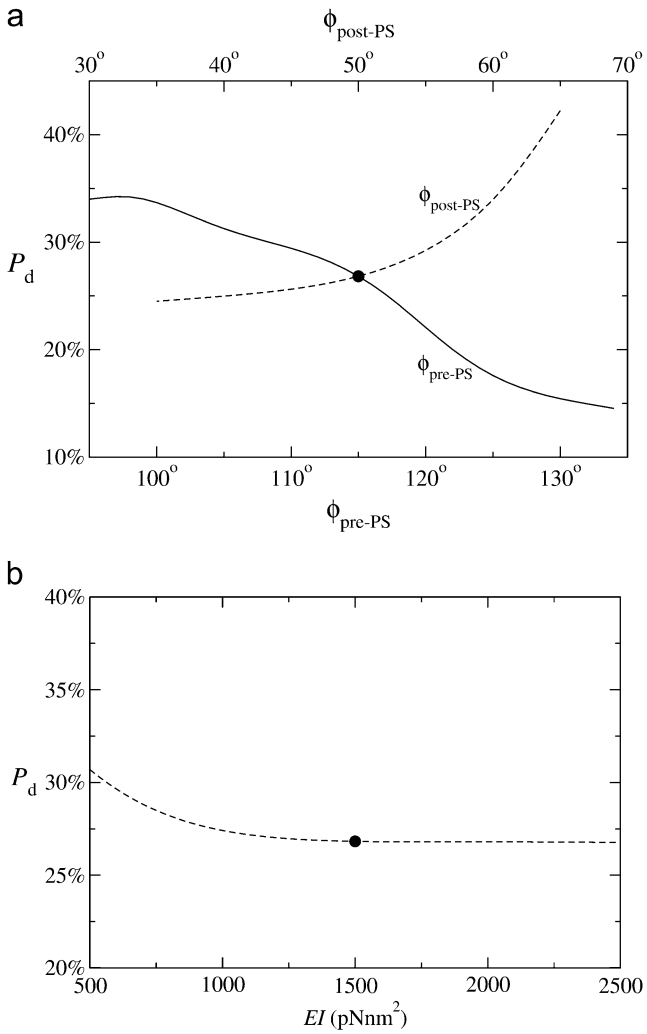

FIGURE 7 Dependence of the calculated branching ratio P_d on different model parameters. (*a*) Dependence on the lead head angle ϕ_{pre-PS} (*solid line*, *lower scale*) and trail head angle $\phi_{post-PS}$ (*dashed line*, *upper scale*). (*b*) Dependence on the lever arm stiffness (bending modulus) *EI*. In both diagrams, the dot shows the value used in all other calculations throughout the article.

I thank Mojca Vilfan for comments on the manuscript and Stan Burgess for helpful discussions.

This work was supported by the Slovenian Research Agency (grant No. P1-0099).

REFERENCES

1. Vale, R. D. 2003. Myosin V motor proteins: marching stepwise towards a mechanism. *J. Cell Biol.* 163:445–450.
2. Sellers, J. R., and C. Veigel. 2006. Walking with myosin V. *Curr. Opin. Cell Biol.* 18:68–73.
3. Rief, M., R. S. Rock, A. D. Mehta, M. S. Mooseker, R. E. Cheney, and J. A. Spudich. 2000. Myosin-V stepping kinetics: a molecular model for processivity. *Proc. Natl. Acad. Sci. USA.* 97:9482–9486.
4. Mehta, A. D., R. S. Rock, M. Rief, J. A. Spudich, M. S. Mooseker, and R. E. Cheney. 1999. Myosin-V is a processive actin-based motor. *Nature.* 400:590–593.
5. Rock, R. S., M. Rief, A. D. Mehta, and J. A. Spudich. 2000. In vitro assays of processive myosin motors. *Methods.* 22:373–381.
6. Veigel, C., F. Wang, M. L. Bartoo, J. R. Sellers, and J. E. Molloy. 2002. The gated gait of the processive molecular motor, myosin V. *Nat. Cell Biol.* 4:59–65.
7. Purcell, T. J., C. Morris, J. A. Spudich, and H. L. Sweeney. 2002. Role of the lever arm in the processive stepping of myosin V. *Proc. Natl. Acad. Sci. USA.* 99:14159–14164.
8. Gebhardt, J. C., A. E. Clemen, J. Jaud, and M. Rief. 2006. Myosin-V is a mechanical ratchet. *Proc. Natl. Acad. Sci. USA.* 103:8680–8685.
9. Clemen, A. E., M. Vilfan, J. Jaud, J. Zhang, M. Barmann, and M. Rief. 2005. Force-dependent stepping kinetics of myosin-V. *Biophys. J.* 88: 4402–4410.
10. Uemura, S., H. Higuchi, A. O. Olivares, E. M. De La Cruz, and S. Ishiwata. 2004. Mechanochemical coupling of two substeps in a single myosin V motor. *Nat. Struct. Mol. Biol.* 11:877–883.
11. De La Cruz, E. M., A. L. Wells, S. S. Rosenfeld, E. M. Ostap, and H. L. Sweeney. 1999. The kinetic mechanism of myosin V. *Proc. Natl. Acad. Sci. USA.* 96:13726–13731.
12. De La Cruz, E. M., A. L. Wells, H. L. Sweeney, and E. M. Ostap. 2000. Actin and light chain isoform dependence of myosin V kinetics. *Biochemistry.* 39:14196–14202.
13. De La Cruz, E. M., H. L. Sweeney, and E. M. Ostap. 2000. ADP inhibition of myosin V ATPase activity. *Biophys. J.* 79:1524–1529.
14. Yengo, C. M., E. M. De la Cruz, D. Safer, E. M. Ostap, and H. L. Sweeney. 2002. Kinetic characterization of the weak binding states of myosin V. *Biochemistry.* 41:8508–8517.
15. Yildiz, A., J. N. Forkey, S. A. McKinney, T. Ha, Y. E. Goldman, and P. R. Selvin. 2003. Myosin V walks hand-over-hand: single fluorophore imaging with 1.5-nm localization. *Science.* 300:2061–2065.

16. Ali, M. Y., S. Uemura, K. Adachi, H. Itoh, K. Kinosita, Jr., and S. Ishiwata. 2002. Myosin V is a left-handed spiral motor on the right-handed actin helix. *Nat. Struct. Biol.* 9:464–467.

17. Forkey, J. N., M. E. Quinlan, M. A. Shaw, J. E. Corrie, and Y. E. Goldman. 2003. Three-dimensional structural dynamics of myosin V by single-molecule fluorescence polarization. *Nature*. 422:399–404.

18. Walker, M. L., S. A. Burgess, J. R. Sellers, F. Wang, J. A. Hammer, J. Trinick, and P. J. Knight. 2000. Two-headed binding of a processive myosin to F-actin. *Nature*. 405:804–807.

19. Burgess, S., M. Walker, F. Wang, J. R. Sellers, H. D. White, P. J. Knight, and J. Trinick. 2002. The prepower stroke conformation of myosin V. *J. Cell Biol.* 159:983–991.

20. Wang, F., K. Thirumurugan, W. F. Stafford, J. A. Hammer, P. J. Knight, and J. R. Sellers. 2003. Regulated conformation of myosin V. *J. Biol. Chem.* 279:2333–2336.

21. Coureux, P. D., A. L. Wells, J. Menetrey, C. M. Yengo, C. A. Morris, H. L. Sweeney, and A. Houdusse. 2003. A structural state of the myosin V motor without bound nucleotide. *Nature*. 425:419–423.

22. Warshaw, D. M., G. G. Kennedy, S. S. Work, E. B. Krementsova, S. Beck, and K. M. Trybus. 2005. Differential labeling of myosin V heads with quantum dots allows direct visualization of hand-over-hand processivity. *Biophys. J.* 88:L30–L32.

23. Baker, J. E., E. B. Krementsova, G. G. Kennedy, A. Armstrong, K. M. Trybus, and D. M. Warshaw. 2004. Myosin V processivity: multiple kinetic pathways for head-to-head coordination. *Proc. Natl. Acad. Sci. USA*. 101:5542–5546.

24. Sakamoto, T., F. Wang, S. Schmitz, Y. Xu, Q. Xu, J. E. Molloy, C. Veigel, and J. R. Sellers. 2003. Neck length and processivity of myosin V. *J. Biol. Chem.* 278:29201–29207.

25. Pantaloni, D., R. Boujemaa, D. Didry, P. Gounon, and M. F. Carlier. 2000. The Arp2/3 complex branches filament barbed ends: functional antagonism with capping proteins. *Nat. Cell Biol.* 2:385–391.

26. Machesky, L. M., R. D. Mullins, H. N. Higgs, D. A. Kaiser, L. Blanchoin, R. C. May, M. E. Hall, and T. D. Pollard. 1999. Scar, a WASp-related protein, activates nucleation of actin filaments by the Arp2/3 complex. *Proc. Natl. Acad. Sci. USA*. 96:3739–3744.

27. Vilfan, A. 2005. Elastic lever-arm model for myosin V. *Biophys. J.* 88:3792–3805.

28. Kolomeisky, A. B., and M. E. Fisher. 2003. A simple kinetic model describes the processivity of myosin-V. *Biophys. J.* 84:1642–1650.

29. Skau, K. I., R. B. Hoyle, and M. S. Turner. 2006. A kinetic model describing the processivity of myosin-V. *Biophys. J.* 91:2475–2489.

30. Vilfan, A., and T. Duke. 2003. Instabilities in the transient response of muscle. *Biophys. J.* 85:818–826.

31. Dunn, A. R., and J. A. Spudich. 2007. Dynamics of the unbound head during myosin V processive translocation. *Nat. Struct. Mol. Biol.* 14: 246–248.

32. Knight, P., and J. Trinick. 1984. Structure of the myosin projections on native thick filaments from vertebrate skeletal muscle. *J. Mol. Biol.* 177:461–482.

33. Offer, G., and P. Knight. 1996. The structure of the head-tail junction of the myosin molecule. *J. Mol. Biol.* 256:407–416.

34. Knight, P. J. 1996. Dynamic behavior of the head-tail junction of myosin. *J. Mol. Biol.* 255:269–274.

35. Egile, C., I. Rouiller, X. P. Xu, N. Volkmann, R. Li, and D. Hanein. 2005. Mechanism of filament nucleation and branch stability revealed by the structure of the Arp2/3 complex at actin branch junctions. *PLoS Biol.* 3:e383.

36. Volkmann, N., K. J. Amann, S. Stoilova-McPhie, C. Egile, D. C. Winter, L. Hazelwood, J. E. Heuser, R. Li, T. D. Pollard, and D. Hanein. 2001. Structure of Arp2/3 complex in its activated state and in actin filament branch junctions. *Science*. 293:2456–2459.

37. Vilfan, A. 2005. Influence of fluctuations in actin structure on myosin V step size. *J. Chem. Inf. Model*. 45:1672–1675.

38. Veigel, C., S. Schmitz, F. Wang, and J. R. Sellers. 2005. Load-dependent kinetics of myosin-V can explain its high processivity. *Nat. Cell Biol.* 7:861–869.

39. Ali, M. Y., E. B. Krementsova, G. G. Kennedy, R. Mahaffy, T. D. Pollard, K. M. Trybus, and D. M. Warshaw. 2007. Myosin Va maneuvers through actin intersections and diffuses along microtubules. *Proc. Natl. Acad. Sci. USA*. 104:4332–4336.

40. Purcell, T. J., H. L. Sweeney, and J. A. Spudich. 2005. A force-dependent state controls the coordination of processive myosin V. *Proc. Natl. Acad. Sci. USA*. 102:13873–13878.

41. Wu, Y., Y. Q. Gao, and M. Karplus. 2007. A kinetic model of coordinated myosin V. *Biochemistry*. 46:6318–6330.

42. Lan, G., and S. X. Sun. 2005. Dynamics of myosin-V processivity. *Biophys. J.* 88:999–1008.

43. Watanabe, T. M., H. Tanaka, A. H. Iwane, S. Maki-Yonekura, K. Homma, A. Inoue, R. Ikebe, T. Yanagida, and M. Ikebe. 2004. A one-headed class V myosin molecule develops multiple large (approximately 32-nm) steps successively. *Proc. Natl. Acad. Sci. USA*. 101: 9630–9635.